

Review

# Photocatalytic Conversion of Biomass over Modified Graphitic Carbon Nitride Catalysts for Environmental Sustainability—A Review

Guangsheng Zhu<sup>1</sup>, Yajie Shu<sup>1,\*</sup>, and Ming Zhou<sup>2,\*</sup><sup>1</sup> National Local Joint Laboratory for Advanced Textile Processing and Clean Production, Wuhan Textile University, Wuhan 430200, China<sup>2</sup> School of Environment and Science, Gold Coast Campus, Griffith University, Gold Coast, QLD 4222, Australia

\* Correspondence: shuyj@mail3@sysu.edu.cn (Y.S.); ming.zhou@griffith.edu.au (M.Z.)

Received: 18 November 2024; Revised: 29 January 2025; Accepted: 15 February 2025; Published: 20 February 2025

**Abstract:** Solar-driven photocatalytic transformations of biomass-derived organic wastes into high-value chemicals and fuels is a crucial and promising strategy for reducing pollution while simultaneously utilizing renewable sources and generating valuable products, contributing to a cleaner and more sustainable environment. However, its efficient conversion remains challenging due to its complex macromolecular structure and the demand for environmentally sustainable processing methods. Graphitic carbon nitride (g-C<sub>3</sub>N<sub>4</sub>) has emerged as a promising photocatalyst for biomass conversion owing to its unique electronic properties, intrinsic stability and structural tunability. This review comprehensively summarizes recent advancements in the modification of g-C<sub>3</sub>N<sub>4</sub>-based photocatalysts for photocatalytic biomass conversion, focusing on strategies including elemental doping, defect engineering, and heterojunction construction. These modifications have enabled efficient conversion of various biomass feedstocks, from simple monosaccharides to complex cellulose structures, while facilitating simultaneous environmental pollution remediation. Furthermore, this review analyses the challenges in improving g-C<sub>3</sub>N<sub>4</sub>-based photocatalysts for biomass photo-reforming and improving the conversion of complex biomass substrates. Finally, by critically evaluating current strategies and highlighting future research directions, this review provides insights for designing advanced g-C<sub>3</sub>N<sub>4</sub>-based photocatalysts for biomass conversion and promotes environmental sustainability.

**Keywords:** biomass; graphitic carbon nitride; heterojunction photocatalysts; environmental sustainability

## 1. Introduction

The escalating global energy crisis of depleting petroleum-based resources and the increasing environmental pollution from organic waste accumulation have intensified the urgency of developing renewable energy sources while mitigating the impact of anthropogenic emissions on ecosystems and ensuring long-term environmental sustainability [1–3]. Biomass, derived from organic materials such as agricultural residues, forestry waste, algae and other organic wastes, has attracted significant attention as a promising alternative to fossil fuels due to its abundance and carbon-neutral nature. It can be converted into biofuels and a variety of value-added chemicals, including ethanol, levulinic acid, 5-hydroxymethylfurfural, and furfural, which are essential in the chemical industry [4–6]. Although biomass mainly consists of three complex polymers, i.e., cellulose, hemicellulose, and lignin [7,8], its intricate composition poses significant challenges to the efficient conversion into valuable chemicals and fuels [9–11]. Sophisticated conversion technologies are required to facilitate efficient conversion with minimal carbon footprint [12,13].

Photocatalysis has emerged as an attractive strategy for both sustainable biomass conversion and pollution remediation, enabling selective chemical transformations while simultaneously addressing environmental contamination concerns [14,15]. Biomass can be converted into fuels and chemicals using a variety of established techniques. Thermochemical methods—such as pyrolysis, gasification, and liquefaction—typically operate at high temperatures and pressures, often resulting in complex mixtures of hydrocarbons or syngas. While pyrolysis can yield bio-oils, char, and gases, the high energy demand and subsequent upgrading steps add complexity and cost to the process [16,17]. Gasification, on the other hand, produces syngas (a mixture of CO and H<sub>2</sub>) that can serve



**Copyright:** © 2025 by the authors. This is an open access article under the terms and conditions of the Creative Commons Attribution (CC BY) license (<https://creativecommons.org/licenses/by/4.0/>).

**Publisher's Note:** Scilight stays neutral with regard to jurisdictional claims in published maps and institutional affiliations.

as a feedstock for Fischer–Tropsch synthesis, but large-scale operation and gas cleanup can be challenging. Biocatalytic (or fermentation-based) methods leverage enzymes or microorganisms to break down biomass, providing high specificity and moderate reaction conditions; however, long reaction times, sensitivity to inhibitors, and extensive pretreatment of lignocellulosic biomass limit industrial feasibility [18,19]. Similarly, thermocatalytic routes [20,21] require harsh reaction conditions or expensive catalysts and can suffer from low selectivity. In recent years, electrocatalysis [22,23] has gained attention for its controllability, but it often necessitates an external power supply and intricate reactor designs. Collectively, these methods underscore the complexity of biomass conversion and the trade-offs in efficiency, selectivity, and sustainability.

In this regard, semiconductor photocatalysis stands out by enabling reactions under mild conditions using abundant solar energy and reducing undesirable by-products. In a typical semiconductor photocatalytic process, photons with energy equal to or greater than the semiconductor's bandgap excite electrons from the valence band to the conduction band, generating electron-hole pairs. These charge carriers migrate to the photocatalyst surface, where they then participate in redox reactions with adsorbed molecules. Efficient separation of electron-hole pairs and effective interaction with reactants are crucial for high photocatalytic activity. The selective conversion of biomass can be achieved through the generation of active free radicals during this process [24,25]. Among various photocatalytic systems, semiconductor materials are particularly significant because of their ability to generate and separate charge carriers upon light absorption, facilitating redox reactions that are essential for biomass conversion. Since Fujishima and Honda's groundbreaking discovery in 1972 of water splitting on titanium dioxide ( $\text{TiO}_2$ ) electrodes under ultraviolet (UV) light [26], semiconductor photocatalysis has gained extensive attention for applications in energy production and environmental remediation. Compared to conventional methods such as pyrolysis [16,17], thermocatalytic conversion [20,21], biocatalysis [18,19] and electrocatalysis [22,23], semiconductor photocatalytic biomass conversion offers several advantages [27,28]. It operates at ambient temperatures and pressures, reduces energy consumption, minimizes the formation of undesirable by-products, and utilizes abundant solar energy [29–31].

The efficiency of semiconductor photocatalytic processes is largely determined by several catalyst characteristics, i.e., the visible-light absorption rate, recombination of photogenerated electron-hole pairs, and active sites [32–35]. To date, traditional semiconductor photocatalysts like  $\text{TiO}_2$  and cadmium sulfide (CdS) have been widely explored but exhibited drawbacks in terms of light absorption capacity and toxicity.  $\text{TiO}_2$  for example, has a large bandgap (~3.2 eV for anatase), restricting its light absorption to the UV region, which accounts for only about 5% of the solar spectrum [36]. Additionally,  $\text{TiO}_2$  suffers from rapid recombination of electron-hole pairs, reducing its photocatalytic efficiency [37]. While CdS, although having a narrower bandgap (2.4 eV) that can absorb visible light, the issues of photo-corrosion and toxicity due to the presence of cadmium making it less suitable for sustainable applications [38]. In this regard, Graphitic carbon nitride (g- $\text{C}_3\text{N}_4$ ) has emerged as a promising semiconductor photocatalyst due to its metal-free nature, environmental compatibility, and visible-light-driven activity, making it an ideal material for mitigating pollution while facilitating resource recovery [39]. As a metal-free, conjugated polymer semiconductor with a two-dimensional layered structure composed of heptazine units linked by nitrogen bridges, g- $\text{C}_3\text{N}_4$  exhibits a moderate bandgap of approximately 2.7 eV, enabling absorption of visible light up to about 460 nm (Figure 1). It is thermally and chemically stable, exhibiting excellent environmental friendliness, and can be synthesised from abundant nitrogen-rich precursors like urea, melamine, and dicyandiamide through simple thermal polymerisation methods [40–42]. To further enhance its performance, various modification strategies were also explored, including optimising the morphology, increasing the specific surface area [43,44], modifying the electronic band structure through element doping [45,46], and introducing defect engineering to alter its electronic properties [47,48]. Additional modification strategies involve the construction of heterojunctions with other semiconductors [49,50], co-catalyst modifications [51,52], and dye sensitisation, all aimed at enhancing photocatalytic activity [53,54].

Given the good tunability of g- $\text{C}_3\text{N}_4$ , its application in the selective conversion of biomass and the mitigation of organic waste accumulation has become increasingly noteworthy. This review explores the latest advances in the application of carbon nitride-based photocatalysts for biomass photoreforming, with a focus on key modification strategies including element doping, defect engineering, and the construction of heterojunctions, which have significantly enhanced the material's light absorption, charge separation efficiency, and catalytic performance, further enabling the effective transformation of organic biomass into value-added chemicals while simultaneously addressing environmental concerns such as organic pollutant degradation. Furthermore, novel approaches, such as donor-acceptor system construction and integration with biocatalysts have been explored to improve charge transfer efficiency and broaden the applicability of g- $\text{C}_3\text{N}_4$ -based photocatalysts in environmental remediation. Moreover, we also discuss how these strategies were applied to achieve selective conversion of various biomass feedstocks, from simple monosaccharides to complex cellulose structures. This work addresses

current challenges in the field, including the demand to integrate both oxidation and reduction reactions in biomass photo reforming to maximise atom utilisation and the difficulties associated with the photocatalytic conversion of complex macromolecular biomass like cellulose. By critically evaluating these approaches and highlighting potential solutions, this work aims to provide new insights for the design and modification of  $g\text{-C}_3\text{N}_4$ -based photocatalysts, ultimately contributing to the development of more efficient biomass conversion technologies for clean energy production, organic pollutant remediation, and environmental sustainability.

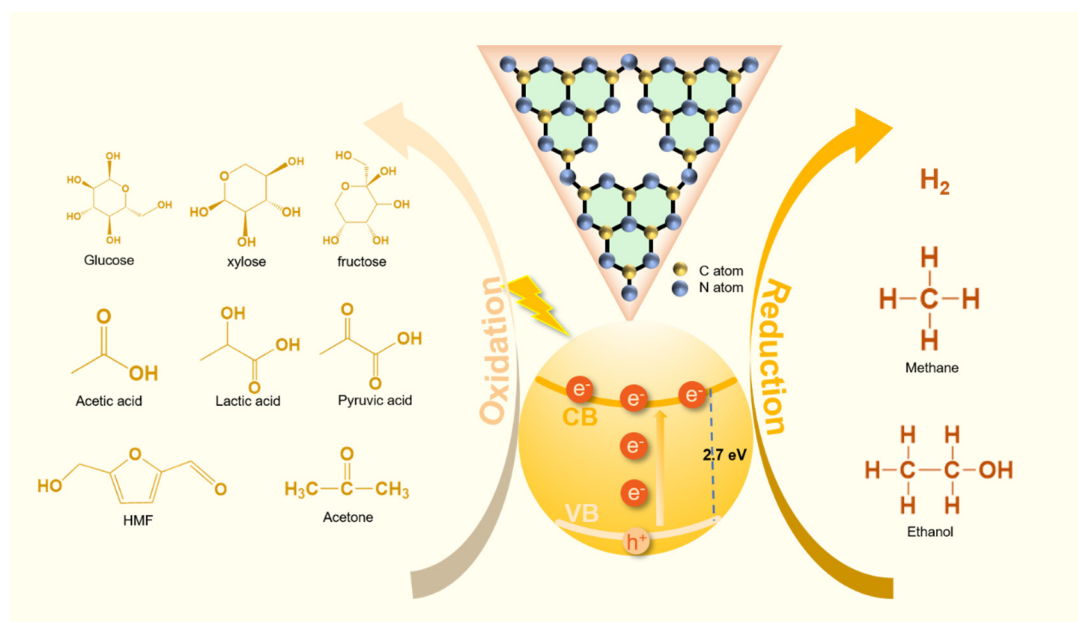


**Figure 1.** Photocatalytic mechanism of carbon nitride and pathways for photocatalytic biomass reforming to produce value-added chemicals.

## 2. Advancements in $g\text{-C}_3\text{N}_4$ Photocatalysts for Biomass Conversion

To date, researchers have been exploring several innovative strategies to boost the activity and selectivity of these catalysts. These include methods like elemental doping to adjust the material's electronic properties, engineering defects to enhance charge separation, and constructing heterojunctions to facilitate better electron flow [55,56]. Additionally, novel approaches such as creating donor-acceptor systems and integrating biocatalysts have shown great promise [57,58]. The following sections delve into these strategies in detail, illustrating how these strategies contribute to more efficient and sustainable conversion of various biomass feedstocks, with key performance summaries in Table 1.

### 2.1. Elemental Doping

Elemental doping refers to the process in which atoms or impurities enter the lattice of  $g\text{-C}_3\text{N}_4$ , either through substituting existing atoms or inserting additional ones. This modification alters the physical and chemical properties of the photocatalyst, leading to an improved photocatalytic performance. By carefully selecting dopant elements, it is possible to reduce the bandgap  $g\text{-C}_3\text{N}_4$ , allowing it to absorb a broader spectrum of visible light. Additionally, elemental doping promotes the delocalization of  $\pi$ -conjugated electrons, which enhances the conductivity, charge carrier mobility, and facilitates the separation of photo-generated electron-hole pairs [59,60]. Based on the type of elements, doping can be classified into metal doping (e.g., Zn, Fe, Pt), non-metal doping (e.g., O, P, B, F, Cl), and metal-nonmetal co-doping.

For example, Ma et al. [61] developed a novel method to prepare Zn-doped carbon nitride (Zn-mCN) with a  $\text{Zn-N}_6$  coordination structure using a calcination-calcination-washing strategy. Compared to carbon nitride, the doping reduced the bandgap from 2.46 eV to 1.80 eV, significantly broadening the absorption range of visible light and lowering the photoluminescence intensity. The Zn-doped catalyst exhibited enhanced photocatalytic redox activity, achieving a lactic acid selectivity of up to 91.0% and a hydrogen production rate of (up to  $15,898.8 \mu\text{mol g}^{-1} \text{h}^{-1}$  during simultaneous biorefinery and water splitting. Similarly, Wang et al. [62] synthesised a Pt-doped polymeric carbon nitride ( $\text{Pt}_x\text{-C}_3\text{N}_4$ ) for cellulose photoreforming via the pyrolysis of a preorganised supramolecular assembly of cyanuric acid, melamine, and  $\text{Pt}(\text{NH}_2\text{-bpy})_2$  (Figure 2a,b). The presence of Pt introduced a surface plasmon effect, which shifted the absorption threshold to longer wavelengths and extended the absorption in the UV-visible

spectrum. Meanwhile, as Pt has a lower work function, electrons are more inclined to migrate to the Pt sites, promoting effective charge separation. The Density functional theory (DFT) calculations confirmed that Pt doping significantly lowered the activation energy barrier for water reduction to hydrogen and facilitated the selective cleavage of the C–C bonds in fructose derived from glucose isomerisation. Another worked conducted by Huang and co-workers [63], who developed a Fe-doped mesoporous graphitic carbon nitride using a simple and economical synthesis approach involving urea and tetraethyl orthosilicate, with iron incorporated to enhance its photocatalytic properties. The introduction of Fe significantly reduced the bandgap, improved visible-light absorption, and promoted efficient separation of electron-hole pairs, resulting in a notable boost in photocatalytic performance. This modified catalyst was effectively applied to selectively cleave C $\alpha$ -C $\beta$  bonds in lignin under mild, visible-light conditions, achieving an impressive 98% conversion rate for a lignin model compound with excellent selectivity. Moreover, it demonstrated strong capability in depolymerising complex dimer model compounds and pine kraft lignin, showcasing high selectivity and adaptability for lignin valorisation.

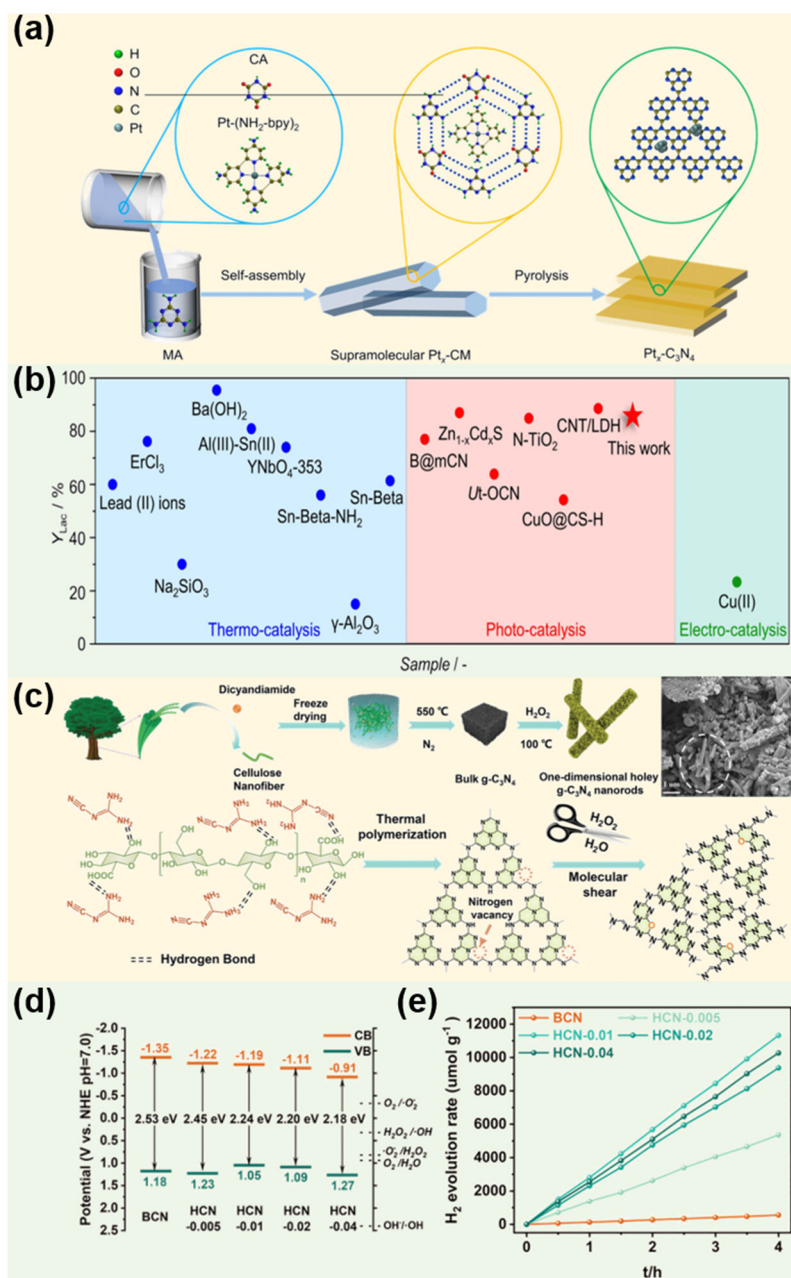


**Figure 2.** (a) Schematic illustration of the preparation of Pt<sub>x</sub>-C<sub>3</sub>N<sub>4</sub>. MA: melamine; CA: cyanuric acid; CM: cyanuric acid-melamine supramolecular complex. (b) Performance map for the catalytic transformation of glucose to lactic acid in various catalytic systems. (c) Illustration of the synthetic route and chemical structure of the nitrogen deficient HCN with oxygen doping. Inset in (c) shows the SEM image of HCN-0.01. (d) Band structure alignments. (e) Photocatalytic H<sub>2</sub> evolution of BCN and HCN.

Non-metal doping is attractive due to its environmental friendliness, as it avoids secondary metal pollution. Wang et al. [64] demonstrated the feasibility of direct cellulose photocatalytic conversion into value-added bioproducts (arabinose) at neutral pH for the first time. They fabricated oxygen-doped carbon nitride (OCN-OH) via a facile solvothermal method using dicyandiamide and cyanuric chloride. Oxygen doping led to greater delocalisation through heteroatom substitution, thus, increasing the charge carrier density. DFT calculations revealed that oxygen-doped g-C<sub>3</sub>N<sub>4</sub> exhibited superior performance in generating arabinose compared to pure g-C<sub>3</sub>N<sub>4</sub>. The proposed mechanism involves oxygen insertion at the C1 position of glucose units within cellulose, leading to oxidative cleavage of β-1,4 glycosidic linkages and the formation of gluconolactone. This intermediate hydrolyses to form gluconic acid, which then decarboxylation via C1–C2 α-scissions to produce arabinose and formic acid. Using cellulose-II as the substrate (1 g/L) at a neutral pH, a conversion rate of approximately 18% was achieved. Combining multiple dopants can further enhance photocatalytic activity by leveraging the benefits of each element. For instance, a spiral-tube-shaped carbon nitride photocatalyst (PACN) with P and O co-doping was prepared by Liu et al. [65] The unique spiral-tube morphology provided more active sites for reactions. P and O co-doping efficiently narrowed the bandgap and broadened the light-harvesting range. Specifically, phosphorus atoms, with their five valence electrons [66], contribute electron-rich sites, while the electron-deficient tri-s-triazine units in g-C<sub>3</sub>N<sub>4</sub> facilitate efficient charge separation, thereby increasing the utilisation efficiency of photo-generated electron-hole pairs and improving the photocatalytic performance.

Metal–nonmetal co-doping is another effective strategy to modify the electronic properties of g-C<sub>3</sub>N<sub>4</sub>. Yang et al. [67] reported a novel K and O co-doped polymeric carbon nitride (K/O@CN-C≡N) with cyano groups incorporated into the structure. The process involved blending urea with diacetylene black and KOH, which melts at 360 °C. During thermal polymerisation, the molten KOH released OH<sup>−</sup> that reacted with the amine groups of the urea-derived intermediate to form cyano groups [68]. The co-doping of K and O atoms modified the electronic structure, narrowed the bandgap, and significantly improved the optical properties, leading to enhanced photocatalytic efficiency.

## 2.2. Defect Engineering

Defect engineering involves the intentional creation and manipulation of imperfections within the crystal structure of g-C<sub>3</sub>N<sub>4</sub> to improve its photocatalytic activity. By introducing defects such as vacancies or dopants, the surface structure and electronic states of the material can be modified, which can result in the enhancement of electron-hole separation, adjusting the band structure, and ultimately improving catalytic activity and selectivity [69]. However, not all defects are beneficial. Certain defects can serve as recombination centres for electron-hole pairs, reducing the overall catalytic performance. Therefore, precise control over defect formation is crucial for optimising photocatalytic properties of g-C<sub>3</sub>N<sub>4</sub>. Defects are typically classified by dimensionality, including point, line, planar, and volume defects, with point defects (vacancies and dopants being the most commonly exploited in modifying carbon nitride [70].

One effective strategy is the introduction of nitrogen vacancies. Ren and co-workers [71] synthesised one-dimensional holey carbon nitride nanorods (HCN) using cellulose nanofibers (CNF) as a soft template and modifier for the photochemical synthesis of lactic acid from monosaccharide photooxidation (Figure 2c). The abundant hydrophilic functional groups on CNFs, such as hydroxy-carboxylic groups, form hydrogen bonds with dicyandiamide during high-temperature pyrolysis. This process leads to condensation reactions that generate a significant number of N vacancies in the carbon nitride structure [72]. These N vacancies enhance visible light absorption and improve the separation of photogenerated electron-hole pairs. The optimised HCN-0.01 catalyst demonstrated excellent performance in the photochemical synthesis of lactic acid from fructose, achieving a 95.5% conversion rate, a 75.5% lactic acid yield and a hydrogen production rate of 2.822 mmol h<sup>−1</sup> g<sup>−1</sup> (Figure 2d,e). Defect engineering can also improve catalytic selectivity. For instance, Bai et al. [73] developed a metal-free photocatalyst (Ce6@BNCN) consisting of nitrogen-deficient carbon nitride (BNCN) and chlorine e6 (Ce6), a photosensitiser, for the efficient and selective oxidation of glucose to gluconic acid and glucaric acid. Pristine carbon nitride was thermally treated with NaBH<sub>4</sub> to obtain BNCN, resulting in a decrease in -NH<sub>2</sub> groups and an increase in N≡C- groups, indicating the formation of two kinds of nitrogen defects [74]. The introduction of nitrogen defects raised the valence band from 1.16 eV to 1.30 eV, enhancing the material's oxidative power. Simultaneously, the surface charge characteristics of BNCN were improved after protonation treatment with hydrochloric acid. Combining BNCN with Ce6 led to a significant redshift in the absorption edge, expanding the light absorption range. DFT calculations showed that Ce6@BNCN catalyst is thermodynamically more favourable for the selectively oxidation of glucose to valuable products like gluconic acid and glucaric acid. In addition to nitrogen defects, another intrinsic defect, carbon defects, can be formed in carbon nitride through the loss of carbon

atoms. It can also improve charge separation and provide additional active sites for reactions. Pure water hydrothermal treatment can partially transform melon-based carbon nitride into a melon-poly (heptazine imide) (PHI) carbon nitride allotropic composite. Chen et al. [75] revealed the intrinsic defects of the presence of carbon vacancies in the melon-PHI carbon nitride allotropic composite by solid-state NMR characterization. The modification of carbon vacancies promotes charge separation in the melon-PHI carbon nitride allotropic composite and enables the parallel processes of hydrogen production from water splitting and the selective oxidation of 5-(hydroxymethyl) furfural to 2,5-diformylfuran, with activities of 41 and 49  $\mu\text{mol g}^{-1} \text{h}^{-1}$ , respectively. In addition to nitrogen and carbon defects, single or multiple defects acting together can improve the catalytic performance of carbon nitride. By introducing  $\text{NaNO}_2$  and  $\text{NH}_3\text{I}$  during the melamine calcination process, a cyano-modified defective carbon nitride (NICN) was successfully constructed by Du and co-workers [76]. Similarly, the introduction of defects also enhanced the light absorption ability of NICN and altered its internal electronic structure, thereby improving its photocatalytic performance. The combined effect of defects, cyano groups, and halogens increased the active sites of NICN and improved the selectivity of glucose conversion to arabinose through a decarboxylation process (with a glucose conversion rate of 91.04% and arabinose yield of 0.262 g/L). Cao et al. [77] prepared ultrathin g- $\text{C}_3\text{N}_4$  with multiple defect sites through a simple self-assembly process and an in-situ thermal gas-shocking/etching process. On one hand, the introduction of defects optimized the electronic structure of g- $\text{C}_3\text{N}_4$ , facilitating charge separation and providing more active photogenerated charge carriers for the reaction. On the other hand, the defects promoted the generation of active free radicals (the activation of  $\text{O}_2$ ) and radical intermediates (C-H activation), which are essential for the reaction. In addition, the multi-defect structure significantly enhanced the cracking performance of the C-C bonds in lignin model compounds.

### 2.3. Constructing Heterojunction

Another effective way to enhance the photocatalytic performance of g- $\text{C}_3\text{N}_4$  is by constructing heterojunctions via the coupling with other semiconductor materials. This strategy expands the range of light absorption, enhances redox capabilities, and optimises electron transport properties by adjusting the band structures of different materials [78,79]. In general, heterojunctions of g- $\text{C}_3\text{N}_4$  are often constructed by coupling carbon with transition metal compounds. For instance, Uekert et al. [80] created a heterojunction catalyst by combining cyanamide-functionalised carbon nitride with a self-prepared nickel phosphide ( $\text{Ni}_2\text{P}$ ), resulting in a low-cost and non-toxic photocatalyst ( $\text{CN}_x|\text{Ni}_2\text{P}$ ). Due to the strong interaction between the  $\text{Ni}_2\text{P}$  and  $\text{CN}_x$ , the intrinsic photocatalytic activity of  $\text{CN}_x|\text{Ni}_2\text{P}$  was greatly enhanced, which promoted its charge separation, catalytic efficiency, and stability. The synthesised catalyst enabling the photocatalytic effectively transformed small organic molecules derived from the hydrolysis of plastics like polyethylene terephthalate and polylactic acid into carbon-based fuels under ambient conditions.

One innovative approach is the construction of S-scheme heterojunctions. These structures consist of a reduction photocatalyst (RP) with a smaller work function and higher Fermi energy level, and an oxidation photocatalyst (OP) with a larger work function and lower Fermi energy level [81]. Unlike traditional heterojunctions, S-scheme heterojunctions effectively separate electron-hole pairs with strong redox capabilities through internal electric fields, band bending, and Coulombic attraction. Ling et al. [82] prepared a sulfur vacancy-enriched heterojunction ( $\text{S}_v$ -rich- $\text{MoS}_2@\text{GCN}$ ) by coupling g- $\text{C}_3\text{N}_4$  with molybdenum disulfide ( $\text{MoS}_2$ ) containing sulfur vacancies. Electron paramagnetic resonance analysis indicated that the formation of  $\text{S}_v$  is probably attributed to the destruction of S atoms during high-temperature annealing [83]. X-ray photoelectron spectroscopy (XPS) showed shifts in binding energies, confirming the formation of an internal electric field and bending associated with the S-scheme heterojunction. DFT calculations further supported these findings. The synergistic effects of  $\text{S}_v$  and the S-scheme significantly improved the catalyst's performance in  $\text{CO}_2$  reduction and selective biomass oxidation without the need for sacrificial agents.

Additionally, g- $\text{C}_3\text{N}_4$  can be coupled with organic semiconductors to form heterojunctions. 3,4,9,10-Perylenetetracarboxylic dianhydride (PDI) is a high-performance n-type organic semiconductor but suffers from charge localisation effects and strong intermolecular aggregation tendencies, limiting its photocatalytic efficiency. Xu and co-workers [84] addressed this issue by constructing an S-Scheme heterojunction (p-CN/P-PDI) (Figure 3a,b). They first grafted polyhedral oligomeric silsesquioxane (POSS) onto both ends of PDI to obtain POSS-PDI, which prevents the crystallisation of PDI on the surface of p-CN while promoting electron conduction. This modified PDI was subsequently coupled with protonated g- $\text{C}_3\text{N}_4$  nanosheets possessing suitable bandgaps and a unique  $\pi$ - $\pi$  conjugated planar structure to get p-CN/P-PDI. The incorporation of POSS-PDI resulted in a smooth film on the g- $\text{C}_3\text{N}_4$  surface, which promoted the rapid complexation of electrons and holes at the heterojunction interface and significantly improved the redox capacity. Meanwhile, an internal electric field was established and the energy

band structure was optimised. The p-CN/P-PDI demonstrated excellent performance in degrading lignin  $\beta$ -O-4 bond model compounds, achieving 99% conversion and 96% selectivity.

In addition to these examples, recent studies have emphasised the importance of robust S-scheme heterojunctions in maximising redox potentials. For instance, Li's group reported a floatable  $\text{Bi}_2\text{WO}_6/\text{C}_3\text{N}_4$  cloth-shaped composite that not only harnesses S-scheme charge transfer for highly efficient pollutant removal but also allows easy recovery in water decontamination [85]. Similarly, an emerging trend involves upgrading classic g- $\text{C}_3\text{N}_4$  to  $\text{C}_3\text{N}_5$ , which exhibits enhanced electronic properties and denser active sites; S-scheme heterojunctions built with  $\text{C}_3\text{N}_5$  have displayed improved photocatalytic performance in both environmental remediation and energy conversion [86]. These findings reveal the potential of designing S-scheme architectures with carefully aligned conduction and valence bands, ensuring spatially separated electrons and holes for strong redox capabilities. From a fabrication perspective, achieving a high-quality interface is crucial, often involving in-situ growth methods or controlled defect formation to anchor one semiconductor onto another. Such strategies help promote charge transfer and reduce interfacial resistance, thereby preventing recombination losses and enhancing overall activity.

Another strategy involves coupling g- $\text{C}_3\text{N}_4$  with solid acid-base catalysts to construct heterojunctions. Ding et al. [87] used a facile wet-chemical approach to synthesize a ternary heterojunction photocatalyst, named NTCN/LDH, by combining g- $\text{C}_3\text{N}_4$  with nitrogen-doped titanium dioxide (N-TiO<sub>2</sub>) and nickel-iron layered double hydroxide (NiFe-LDH). The NiFe-LDH provided Lewis acid sites that selectively adsorb sugars like glucose and fructose, significantly enhancing sugar isomerisation. The constructed heterojunction not only enhanced charge separation but also facilitated selective cleavage of C-C bonds by generating superoxide radicals ( $\text{O}_2^-$ ), leading to desired products. The integration of thermal and photocatalysis enabled NTCN/LDH to convert glucose to lactic acid at 60 °C with 99% yield (Figure 3c,d), overcoming the limitations of traditional methods that require expensive microbes, long production cycles and high reaction temperature, which also addressing purification challenges associated with conventional catalysts.

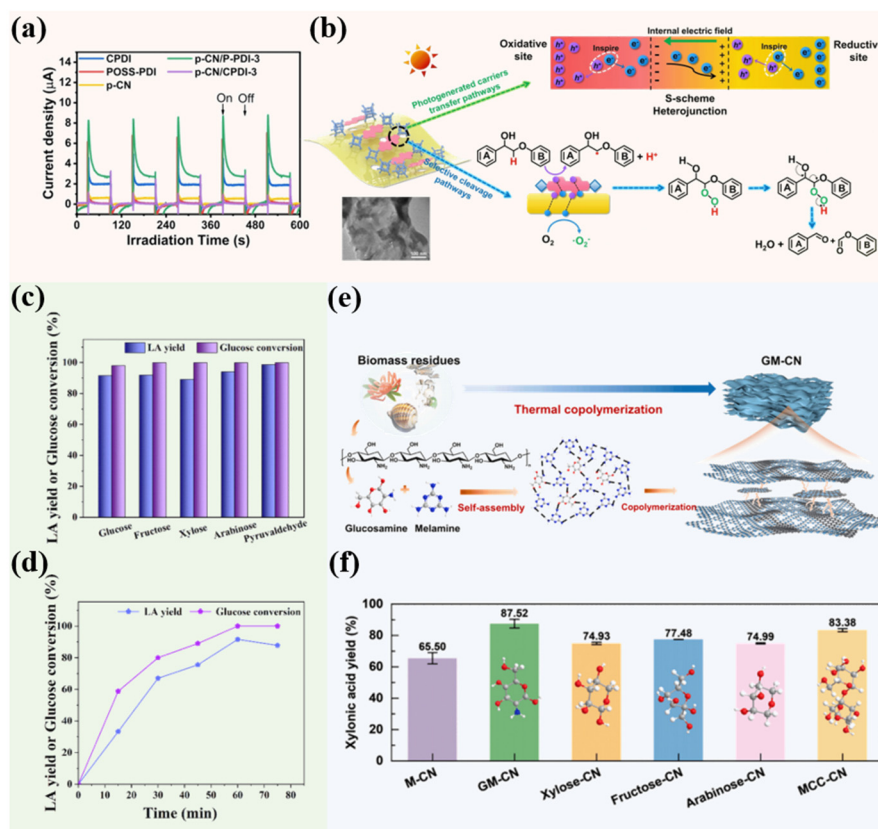


**Figure 3.** (a) Transient photocurrent response of different samples. (b) Proposed mechanism of photocatalytic selective cleavage of the  $\beta$ -O-4 model over p-CN/P-PDI S-scheme heterojunction. Inset in (b) shows the TEM image of p-CN/P-PDI-3. (c) Influence of diverse substrates on the synthesis of LA. (d) reaction times on the synthesis of LA from glucose. (e) Synthesis and morphology structure of GM-CN. (f) the photocatalytic performance when employing different biomass micro-molecules as the carbon source.

## 2.4. Others

In addition to enhancing visible light absorption and photogenerated electron-hole separation through strategies like elemental doping, defects engineering and heterojunctions construction, researchers have explored other novel structures and combinations to boost the photocatalytic performance of g-C<sub>3</sub>N<sub>4</sub>. Two notable strategies are the development of donor-acceptor (D-A) systems and the integration of biocatalysts, both of which have shown significant promise in improving efficiency and selectivity in biomass conversion processes.

D-A systems are gaining attention attributing to their abilities to significantly improve charge transfer within photocatalysts [88,89]. By reducing the potential barriers for electron hopping and facilitating electron shuttle, these systems suppress the recombination of photoinduced electron-hole pairs, leading to enhanced photocatalytic activity [90,91]. Liu et al. [92] demonstrated this by constructing a biochar-welded D-A system within carbon nitride, denoted as GM-CN (Figure 3e,f). The synthesis was achieved by combining glucosamine (GM)-derived carbocyclic ring (the donor) with the planar tri-s-triazine units (the acceptor) through sp<sup>2</sup>-hybridised C-N bonds using multi-step thermal polymerisation. This D-A structure generated an intrinsic driving force that promotes  $\pi$ -electron delocalisation and increases the degree of conjugation within the material. DFT calculations indicated that the exciton binding energy of GM-CN decreased from 208.21 meV to 119.62 meV, indicating its excellent performance in facilitating rapid separation of photoinduced electron-hole pairs [93]. Additionally, the introduction of the D-A structure reduced the band gap of the pristine carbon nitride from 2.71 eV to 2.48 eV, allowing the material to absorb a broader spectrum of light. Furthermore, the intermolecular  $\pi$ - $\pi$  stacking within the D-A system also provides pathways for electrons to migrate toward the catalyst surface. As a result, GM-CN achieved an impressive 87.52% yield of xylonic acid in the photocatalytic oxidation of xylose.

Another innovative approach involves creating hybrid structures that combine g-C<sub>3</sub>N<sub>4</sub> with other materials to enhance light absorption and charge separation. A representative work was done by Ling and co-workers [94] who used ultrasonic-assisted self-assembly and evaporation-drying strategy to incorporate carbon nitride nanosheets onto the surface of C. I. Pigment Yellow 53 (TiO<sub>2</sub>-NiO-Sb<sub>2</sub>O<sub>3</sub>, PY53) to prepare a photocatalyst, named CNs@PY53-x. Attributing the excellent visible light absorption ability and a rutile-type crystal structure with TiO<sub>2</sub> of PY53, the synthesised CNs@PY53 exhibited an abundant mesoporous structure with a large specific surface area. The interfacial interaction between CNs and PY53 narrowed the bandgap of CNs@PY53-2 to 1.53 eV, which significantly enhances its ability to absorb visible light. Photoelectrochemical measurements revealed that CNs@PY53-2 exhibited higher photocurrent density and lower resistance compared to its individual components, indicating improved charge separation of photogenerated electron-hole pairs. When tested in the xylose-alkaline system, CNs@PY53-2 achieved a lactate yield of 86.9% and a CO evolution rate of 371.56  $\mu\text{mol g}^{-1} \text{h}^{-1}$ , demonstrating its effectiveness in biomass conversion applications.

Biocatalysts offer highly specific biological catalytic power and regeneration capabilities, which can complement the properties of semiconductor photocatalysts. By integrating biocatalysts with g-C<sub>3</sub>N<sub>4</sub>, researchers can address some of the limitations of traditional photocatalytic systems, such as low selectivity and the need for harsh reaction conditions [95–97]. Ye et al. [98] explored this by constructing a bio-abiotic photocatalytic system aimed at converting plastic waste to fuel. In their work, a precursor was first obtained by synthesising carbon dots via hydrothermal treatment of  $\alpha$ -cellulose. These carbon dots were subsequently calcined with melamine and KSCN to produce carbon dot-functionalised polymeric carbon nitrides (CDPCN). The incorporation of carbon dots adjusted the oxidation potential of polymeric carbon nitrides to meet the specific requirements of oxidating microplastics and enhanced charge separation capabilities. Subsequently, the CDPCN was then combined with *Methanosarcina barkeri* (*M. b*), a type of methanogenic archaea, to form biohybrids referred to as *M. b*-CDPCN. The CDPCN was attached tightly to the *M. b* surface through electrostatic interactions. In this system, the conversion of microplastics to CH<sub>4</sub> occurred via two parallel pathways. i.e., photo-oxidative methanogenesis (conversion to CH<sub>4</sub> via pyruvate/acetate of the active substance) and photo-reductive methanogenesis (CO<sub>2</sub>-CH<sub>4</sub> conversion via photo-excited electrons). Notably, this process does not require chemical sacrificial agents. The self-assembled *M. b*-CDPCN biohybrids achieved sustainable production of high-purity CH<sub>4</sub> (>99.5%), showcasing the potential of combining biocatalysts with photocatalysts for efficient biomass conversion and waste recycling. Another biocatalyst was developed by Shangguan et al. [99], who covalently immobilised *Candida antarctica* lipase B (CALB) onto functionalized graphitic carbon nitride nanosheets (g-C<sub>3</sub>N<sub>4</sub>-Ns), modified with polyethyleneimine (PEI) and glutaraldehyde (GA). This functionalisation improved enzyme stability, thermal resistance, and catalytic efficiency, enhancing performance under various reaction conditions. The biocatalyst was employed for the esterification of lutein with succinic anhydride in dimethylformamide (DMF), achieving an esterification rate of up to 92% within 60 h. Compared to free CALB, the immobilized enzyme demonstrated significantly greater conversion efficiency and reusability, maintaining a high rate even after multiple cycles.

Similarly, Xu et al. [100] developed a hybrid system by coupling graphitic carbon nitride (g-C<sub>3</sub>N<sub>4</sub>) with *Ralstonia eutropha* to stimulate polyhydroxybutyrate (PHB) production under visible light. This integration facilitated the transfer of reducing power from g-C<sub>3</sub>N<sub>4</sub> to the bacterial cells, enhancing energy metabolism and PHB biosynthesis. The system was applied to bioplastic production from fructose, showing a 1.2-fold increase in PHB production without a sacrificial electron donor and a 1.4-fold increase when triethanolamine was added. The hybrid setup demonstrated a significant boost in PHB yield compared to controls, leveraging light-driven energy transfer to improve microbial productivity.

Recently, Wang et al. [101] utilised a hybrid photosynthesis system combining g-C<sub>3</sub>N<sub>4</sub> with *Cupriavidus necator* to enhance the production of polyhydroxybutyrate from fructose under visible light. This approach optimized conditions such as light intensity, aeration, and inoculum size to maximize efficiency. The system was applied for bioplastic production, leveraging light-driven reducing equivalents to boost microbial synthesis. The optimized hybrid system achieved a PHB production rate of 7.16 g/L/day with a 60.94% yield, significantly outperforming previous setups under higher light intensity.

**Table 1.** Summary of photocatalytic biomass conversion using modified g-C<sub>3</sub>N<sub>4</sub>-based photocatalysts.

| Modifying Strategies   | Biomass Substrate                | Synthesised Photocatalyst  | Product                                    | Conversion Rate   | Yield   | References |
|--|----------------------------------|--|--|---|---|------------|
| Zn doping  | Pentoses, Hexoses                | Zn-doped g-C <sub>3</sub> N <sub>4</sub> (Zn-mCN)                          | Lactic acid, Hydrogen                      | --  | 91% (Lactic acid)   | [61]       |
| Pt doping  | Lignocellulose (Glucose, etc.)   | Pt-doped polymeric carbon nitride  | Hydrogen, Lactic acid                      | 100% (Glucose)  | 86% (Lactic acid)   | [62]       |
| Fe doping  | Lignin                           | Fe-doped mesoporous g-C <sub>3</sub> N <sub>4</sub> (Fe/mpg-CN)            | Aromatic compounds                         | 98%   | 98% (C $\alpha$ -C $\beta$ bonds)   | [63]       |
| O doping   | Cellulose                        | Oxygen-doped g-C <sub>3</sub> N <sub>4</sub>                               | Arabinose, Formic acid                     | ~18%  | -   | [64]       |
| P/O Co-doping  | Monosaccharides                  | P/O Co-doped hollow-tube-shaped g-C <sub>3</sub> N <sub>4</sub>            | Lactic acid, Hydrogen                      | -   | 93.0% (Lactic acid)   | [65]       |
| K/O Co-doping  | Xylose, Pentoses, Hexoses        | K/O Co-doped g-C <sub>3</sub> N <sub>4</sub>                               | Lactic acid, Hydrogen                      | ~95% (Xylose)   | 90.5% (Lactic acid)   | [67]       |
| Engineering Defects (Nitrogen Vacancies + Oxygen Dopants)      | Monosaccharides                  | 1D Holey Carbon Nitride Nanorods (HCN)                                     | Lactic acid, H <sub>2</sub>                | -   | 75.5% (Lactic acid)   | [71]       |
| Engineering Defects + Ce6 Modification                         | Glucose                          | Ce6-modified nitrogen-deficient g-C <sub>3</sub> N <sub>4</sub> (Ce6@BNCN) | Gluconic acid, Glucaric acid               | 62.3%   | 70.9% (Total selectivity)   | [73]       |
| Engineering Defects (Carbon vacancies)                         | H <sub>2</sub> O<br>5-HMF        | Melon- PHI with carbon vacancies carbon nitride allotropic composite       | H <sub>2</sub><br>2,5-diformylfuran        | -   | 41 $\mu\text{mol g}^{-1} \text{h}^{-1}$ with (TEOA and Pt)<br>49 $\mu\text{mol g}^{-1} \text{h}^{-1}$ | [75]       |
| Engineering Defects (Single defects)                           | Glucose                          | Cyano-modified defective carbon nitride (NICN)                             | Arabinose                                  | 91.04%  | The yield of arabinose reaches 0.262 g/L  | [76]       |
| Engineering Defects (multiple defects)                         | Lignin $\beta$ -O-4 model        | Ultrathin g-C <sub>3</sub> N <sub>4</sub> with multiple defective sites    | Aromatic compounds                         | -   | 102% increase in C-C cleavage activity and 90% selectivity  | [77]       |
| Cyanamide-functionalized carbon nitride with Ni <sub>2</sub> P | PET and PLA (plastic substrates) | CNx   Ni <sub>2</sub> P  | H <sub>2</sub> and organic chemicals       | Maintained conversion efficiency on upscaling                   | -   | [80]       |
| Constructing S-scheme heterojunction                           | Xylose                           | S <sub>v</sub> -MoS <sub>2</sub> @GCN                                      | Xylonic acid                               | CO evolution rate of 68.3 $\mu\text{mol g}^{-1} \text{h}^{-1}$  | 64.2%   | [82]       |
| Constructing S-scheme heterojunction                           | Lignin $\beta$ -O-4 model        | p-CN/P-PDI   | Aromatic compounds                         | 16.42-fold increase in conversion compared to initial materials | 35-fold increase in selective cleavage yield  | [84]       |
| Constructing Ternary heterojunctions                           | Glucose, Fructose, Xylose        | g-C <sub>3</sub> N <sub>4</sub> /N-TiO <sub>2</sub> /NiFe-LDH              | Lactic Acid                                | Up to 99%   | 92%   | [87]       |
| Donor-acceptor systems   | Xylose                           | g-C <sub>3</sub> N <sub>4</sub> with biochar-welded D-A structure (GM-CN)  | Xylonic Acid<br>Formic acid<br>Lactic acid | -   | 87.52%<br>26.91%<br>5.55%   | [92]       |
| Hybrid structures  | Xylose                           | CNs@PY53-2   | CO and Lactic Acid                         | --  | 86.9% (lactic acid)   | [94]       |

**Table 1. Cont.**

| Modifying Strategies   | Biomass Substrate                                      | Synthesised Photocatalyst   | Product                    | Conversion Rate            | Yield                             | References |
|--|--|---|----------------------------|----------------------------|-----------------------------------|------------|
| Methanosarcina barkeri on g-C <sub>3</sub> N <sub>4</sub>      | Poly (lactic acid) and non-biodegradable microplastics | g-C <sub>3</sub> N <sub>4</sub> with M. barkeri                             | Methane (CH <sub>4</sub> ) | 90.2% mineralization (PLA) | 99.1% CH <sub>4</sub> selectivity | [98]       |
| Candida antarctica lipase B on g-C <sub>3</sub> N <sub>4</sub> | Lutein   | g-C <sub>3</sub> N <sub>4</sub> functionalized with PEI-GA immobilized CALB | Lutein esters              | 92%                        | -                                 | [99]       |
| Ralstonia eutropha on g-C <sub>3</sub> N <sub>4</sub>          | Fructose   | g-C <sub>3</sub> N <sub>4</sub> with R. eutropha                            | Polyhydroxybutyrate (PHB)  | -                          | 1.4 times increase (with TEOA)    | [100]      |
| Cupriavidus necator on g-C <sub>3</sub> N <sub>4</sub>         | Fructose   | g-C <sub>3</sub> N <sub>4</sub> with C. necator                             | Polyhydroxybutyrate (PHB)  | -                          | 60.94% PHB yield from fructose    | [101]      |

### 2.5. Comparison of g-C<sub>3</sub>N<sub>4</sub> Modification Strategies

To date, research on g-C<sub>3</sub>N<sub>4</sub> modification has primarily focused on strategies such as elemental doping, defect engineering, heterojunction construction, donor–acceptor systems, and biocatalyst integration. Each approach provides distinct benefits but also entails certain limitations, as summarised in Table 2. For instance, elemental doping effectively extends the visible-light absorption range and introduces new active sites for catalysis, yet maintaining uniform dopant distribution poses a challenge at larger scales [59,60]. Similarly, defect engineering enhances charge separation and catalytic specificity by introducing vacancies, but overly high defect densities can foster recombination centres or compromise structural integrity [69,70,74,77]. Constructing heterojunctions, whether S-scheme or conventional type-II, optimises charge transport and broadens the absorption spectrum. Nonetheless, synthesising robust heterojunctions can require complex procedures and the use of costly secondary materials [78–80,87]. D–A systems help lower exciton binding energy and promote selective redox processes, but designing stable D–A architectures often involves multiple synthetic steps and precise alignment of donor–acceptor moieties [88–92]. Finally, integrating biocatalysts confers high specificity under mild conditions, albeit with the risk of enzyme or microbial deactivation under prolonged irradiation and potential toxicity from doping components [95–99].

**Table 2.** Comparison of common modification strategies for g-C<sub>3</sub>N<sub>4</sub>-based photocatalysts.

| Modification Strategy  | Advantages   | Disadvantages  |
|--|--|--|
| Elemental Doping (Metal or Non-Metal)                          | <ul style="list-style-type: none"> <li>Tailors the band structure to broaden visible-light absorption;</li> <li>Can create new active sites and reduce exciton recombination;</li> <li>Potentially enhances selectivity for specific biomass substrates.</li> </ul>                            | <ul style="list-style-type: none"> <li>Possible dopant leaching under prolonged use (especially metal doping);</li> <li>Uniform doping is challenging at large scale;</li> <li>Overdoping can introduce new recombination centers.</li> </ul>                                      |
| Defect Engineering (e.g., Nitrogen or Carbon Vacancies)        | <ul style="list-style-type: none"> <li>Enhances charge-carrier separation by forming localised energy states;</li> <li>Improves targeted bond cleavage in biomass molecules;</li> <li>Can be metal-free, avoiding secondary pollution.</li> </ul>  | <ul style="list-style-type: none"> <li>Defect concentration and type can be difficult to control;</li> <li>Certain defects may act as recombination centers if poorly managed;</li> <li>High defect loading may compromise long-term structural stability.</li> </ul>              |
| Heterojunction Construction (Conventional Type-II or S-Scheme) | <ul style="list-style-type: none"> <li>Promotes spatial separation of photogenerated e<sup>-</sup>/h<sup>+</sup> pairs, increasing redox efficiency;</li> <li>Potentially extends visible-light absorption range;</li> <li>Can reduce or eliminate the need for sacrificial agents.</li> </ul> | <ul style="list-style-type: none"> <li>Complex synthesis and interfacial engineering are required;</li> <li>Secondary semiconductors or co-catalysts can be expensive.</li> <li>Band alignment must be precisely tuned.</li> </ul>   |
| Donor–Acceptor (D–A) Systems                                   | <ul style="list-style-type: none"> <li>Lowers exciton binding energy, facilitating charge separation;</li> <li>Enhances π-electron delocalisation and improves selectivity in redox reactions.</li> </ul>  | <ul style="list-style-type: none"> <li>Requires careful selection and design of donor/acceptor moieties.</li> <li>Increased synthetic complexity and cost.</li> <li>Structural stability may be sensitive to harsh reaction conditions</li> </ul>                                  |
| Integration with Biocatalysts (Enzymes, Microbes)              | <ul style="list-style-type: none"> <li>High specificity for target products (e.g., fine chemicals);</li> <li>Operates under mild reaction conditions (near-neutral pH, moderate temperature);</li> <li>Potential for tandem processes (photocatalysis + biocatalysis).</li> </ul>              | <ul style="list-style-type: none"> <li>Biomolecules can be inactivated by prolonged light or extreme pH;</li> <li>Possible toxicity of dopants or catalyst materials to living cells;</li> <li>Enzyme loading, reusability, and long-term stability may be challenging.</li> </ul> |

In practice, researchers often employ a combination of these modifications to achieve synergetic improvements in photocatalytic performance, especially when targeting complex biomass feedstocks or diverse product streams. Despite these advancements, significant hurdles remain in scaling up production, maintaining long-term stability, and addressing the recalcitrant nature of biomass. Consequently, continued efforts to tackle

these overarching challenges are crucial for realising the full potential of g-C<sub>3</sub>N<sub>4</sub>-based photocatalysts in sustainable biomass conversion.

### 3. Challenges in Enhancing g-C<sub>3</sub>N<sub>4</sub> Photocatalysts for Biomass Conversion

Despite progress in developing various kinds of modified carbon nitride for biomass conversion, several challenges remain. One major issue is the insufficient integration of oxidation and reduction half-reactions during photocatalysis. Current research often emphasizes either hydrogen production (reduction) or the synthesis of value-added chemicals (oxidation) without fully combining both processes. This separation results in inefficient utilisation of atomic resources and limits the overall efficiency of the system [102,103]. Developing photocatalysts that can simultaneously facilitate both half-reactions with high selectivity and efficiency remains a significant challenge.

Another substantial obstacle is the complex nature of biomass substrates such as cellulose and lignin, which impedes high selectivity and efficiency in their conversion. These macromolecules possess intricate and recalcitrant structures, making it difficult to selectively target specific bonds or functional groups. The rigid crystalline structure of cellulose and the heterogeneous, highly branched architecture of lignin limit the accessibility of active sites on the photocatalyst. Consequently, photocatalytic conversion often yields low conversion rates and a mixture of products, complicating downstream processing. Furthermore, the variability of cellulose derived from different sources and pretreatment methods adds another layer of complexity to its interaction with photocatalysts, often leading to inconsistent performance and selectivity [104].

Furthermore, the specific hurdles in photocatalytic biomass conversion vary considerably based on the target products. For instance, the production of biofuels (e.g., hydrogen, bio-oil precursors) typically requires high throughput, robust catalyst stability, and consistent performance over large volumes of feedstock. Achieving high conversion efficiency under mild conditions can be difficult, especially when dealing with unrefined lignocellulosic biomass. The synthesis of platform chemicals (such as 5-hydroxymethylfurfural (HMF), furfural, levulinic acid, or lactic acid) demands excellent selectivity [105,106]. Partial or over-oxidation of intermediates can lead to undesired side products or catalyst deactivation. The wide range of functional groups in biomass molecules increases the likelihood of parallel reactions, making it challenging to preserve catalyst integrity and maintain yield over multiple cycles. Fine chemicals, on the other hand, typically have lower volume but higher value. They often require multi-step transformations under mild, carefully controlled conditions to preserve complex functional groups. In such processes, even minor deviations in reaction parameters can result in significant yield losses, further complicating catalyst design and reaction optimisation [107,108]. Moreover, the presence of various phenolic and carbohydrate structures in biomass feedstocks can deactivate or foul active sites, demanding sophisticated engineering of the photocatalyst surface. Addressing these product-specific challenges requires precise control over redox potentials, functional-site engineering, and reactor design. At the same time, efforts to tailor the catalyst for each desired product type must also be reconciled with the broader concerns of scalability and cost-effectiveness, which remain formidable obstacles to the practical deployment of modified g-C<sub>3</sub>N<sub>4</sub> materials.

The scalability and cost-effectiveness of synthesis methods for modified g-C<sub>3</sub>N<sub>4</sub> materials also present significant challenges. Many enhancement strategies—such as precise elemental doping, controlled defect engineering, and the construction of complex heterojunctions—involve intricate procedures that are difficult to replicate on an industrial scale. Achieving uniform doping or defect distribution necessitates meticulous control over synthesis conditions, which may not be feasible for large-scale production. Additionally, some modification methods utilize rare or expensive elements like platinum or require multi-step synthesis processes, increasing overall costs and limiting commercial viability. Therefore, developing cost-effective and scalable synthesis methods using abundant and non-toxic materials is essential to overcome this obstacle.

Ensuring the stability and durability of modified g-C<sub>3</sub>N<sub>4</sub> photocatalysts under operational conditions constitutes another significant hurdle. Photocatalytic reactions often occur in harsh environments, including exposure to strong oxidising or reducing agents, extreme pH values, and prolonged light irradiation—all of which can lead to photocorrosion or structural degradation of the catalyst. For instance, metal-doped photocatalysts may suffer from metal leaching, diminishing their activity over time and posing environmental risks due to metal contamination. Similarly, integrating biocatalysts introduces concerns regarding the compatibility and stability of biological components within photocatalytic systems, such as enzyme denaturation or microbial viability under reaction conditions. Maintaining long-term stability without sacrificing catalytic performance remains critical for practical applications.

#### 4. Conclusions and Future Perspectives

The photocatalytic conversion of biomass provides a sustainable route for clean fuel and high-valued chemical production and serves as an effective strategy for environmental pollution control, particularly in addressing organic waste accumulation.  $g\text{-C}_3\text{N}_4$  has emerged as a highly promising photocatalyst in this field due to its visible light absorption capabilities by converting the abundant solar energy into chemical energy, chemical stability, and ease of synthesis from abundant materials. This review has summarized recent advancements in enhancing the photocatalytic performance of  $g\text{-C}_3\text{N}_4$  through strategies including elemental doping, defect engineering, heterojunction construction, and innovative approaches like donor–acceptor systems and biocatalyst integration. These modifications have enabled the effective conversion of a wide range of biomass feedstocks from simple sugars to complex cellulose structures, reducing environmental risks associated with uncontrolled biomass decomposition. However, challenges persist, including the scalability of synthesis techniques, the stability of photocatalysts under operational conditions, and the effective conversion of structurally complex biomass substrates.

Future research should focus on addressing these challenges to fully realize the potential of  $g\text{-C}_3\text{N}_4$  photocatalysts in practical applications. One of the most critical research directions is the development of photocatalysts capable of simultaneously driving both oxidation and reduction reactions. Achieving this balance is essential to maximize atom economy, improve overall energy efficiency, and expand the applicability in waste-to-energy conversion and pollution mitigation. Moreover, designing  $g\text{-C}_3\text{N}_4$  materials with tailored band structures and active sites that facilitate synergistic half-reactions could significantly enhance performance. A major challenge in biomass conversion is the efficient breakdown of complex macromolecular biomass such as cellulose and lignin, which exhibit high recalcitrance and structural heterogeneity. Overcoming this limitation may require modifying the surface properties and morphology of  $g\text{-C}_3\text{N}_4$  to improve substrate interaction, introducing functional groups to enhance catalytic selectivity, and engineering hierarchical porous structures to increase active site accessibility. Future efforts should be directed towards developing scalable and environmentally friendly synthesis methods, utilizing abundant and non-toxic elements for doping, and simplifying fabrication processes that minimize environmental impact. Ensuring the stability and durability of  $g\text{-C}_3\text{N}_4$  under operational conditions is also crucial, which may involve designing robust structures or protective coatings to prevent degradation. Additionally, advancing the understanding of photocatalytic mechanisms through sophisticated characterisation techniques and theoretical modelling will guide the rational design of more efficient and selective catalysts. Addressing these challenges will enable the development of more efficient, sustainable, and economically viable biomass conversion technologies using  $g\text{-C}_3\text{N}_4$ -based photocatalysts, thereby contributing to clean energy production, pollutant remediation, and global environmental sustainability.

Moving forward, more specialised catalyst designs and larger-scale testing will be essential to translate laboratory successes into industrial applications. For instance, ribbon-like or fibrous  $g\text{-C}_3\text{N}_4$  architectures could simplify recovery in water purification processes by combining high surface areas with straightforward separation methods. Scalable production strategies and techno-economic assessments are needed to confirm the feasibility of these novel architectures at commercial scales. Furthermore, integrating advanced in situ diagnostic tools can provide real-time insights into catalyst stability and performance, ensuring that oxidation and reduction reactions are systematically optimized for practical applications. Although co-catalyst modifications have proven successful in other photocatalytic fields (e.g., water splitting), their direct application to  $g\text{-C}_3\text{N}_4$ -based biomass conversion is relatively unexplored. Tailoring co-catalyst strategies to specific biomass substrates may unlock new pathways for improving selectivity and reaction efficiency, ultimately paving the way for high-performance  $g\text{-C}_3\text{N}_4$ -based biorefineries. By advancing material design, improving process scalability, and deepening the understanding of reaction mechanisms,  $g\text{-C}_3\text{N}_4$ -based photocatalysis can play a transformative role in sustainable energy production, waste valorization, and environmental remediation.

**Author Contributions:** G.Z.: Data curation, Writing—original draft preparation; Y.S.: Investigation, Writing—editing & proofreading, Supervision; M.Z.: Supervision, Writing—review, editing. All authors have read and agreed to the published version of the manuscript.

**Funding:** This research was funded by the Australian Research Council Early-Career Industry Fellowship, grant number IE230100593.

**Institutional Review Board Statement:** Not applicable.

**Informed Consent Statement:** Not applicable.

**Data Availability Statement:** Not applicable.

**Conflicts of Interest:** The authors declare no conflict of interest.

## References

1. Achakulwisut, P.; Erickson, P.; Guivarch, C.; Schaeffer, R.; Brutschin, E.; Pye, S. Global fossil fuel reduction pathways under different climate mitigation strategies and ambitions. *Nat. Commun.* **2023**, *14*, 5424.
2. Liao, Y.; Koelewijn, S.-F.; Van den Bossche, G.; Aelst, J.V.; Van den Bosch, S.; Renders, T.; Navare, K.; Nicolai, T.; Aelst, K.V.; Maesen, M.; et al. A sustainable wood biorefinery for low-carbon footprint chemicals production. *Science* **2020**, *367*, 1385–1390.
3. Wang, T.; Zhou, T.; Li, C.; Song, Q.; Zhang, M.; Yang, H. Development status and prospects of biomass energy in China. *Energies* **2024**, *17*, 4484.
4. Zhao, H.; Liu, J.; Zhong, N.; Larter, S.; Li, Y.; Kibria, M.G.; Su, B.L.; Chen, Z.; Hu, J. Biomass photoreforming for hydrogen and value-added chemicals co-production on hierarchically porous photocatalysts. *Adv. Energy Mater.* **2023**, *13*, 2300257.
5. Ghalt, R.; Chauhan, A.; Srivastava, R. Heterogeneous photocatalytic valorization of lignocellulose biomass for chemical and fuel production via reductive pathways. *Sustain. Energy Fuels* **2024**, *8*, 3205–3246.
6. Wu, X.; Luo, N.; Xie, S.; Zhang, H.; Zhang, Q.; Wang, F.; Wang, Y. Photocatalytic transformations of lignocellulosic biomass into chemicals. *Chem. Soc. Rev.* **2020**, *49*, 6198–6223.
7. Zavrel, M.; Bross, D.; Funke, M.; Büchs, J.; Spiess, A.C. High-throughput screening for ionic liquids dissolving (ligno-)cellulose. *Bioresour. Technol.* **2009**, *100*, 2580–2587.
8. Zhao, H.; Li, C.-F.; Yu, X.; Zhong, N.; Hu, Z.-Y.; Li, Y.; Larter, S.; Kibria, M.; Hu, J. Mechanistic understanding of cellulose  $\beta$ -1,4-glycosidic cleavage via photocatalysis. *Appl. Catal. B* **2022**, *302*, 120872.
9. Song, W.; Liu, H.; Zhang, J.; Sun, Y.; Peng, L. Understanding H $\beta$  zeolite in 1,4-dioxane efficiently converts hemicellulose-related sugars to furfural. *ACS Catal.* **2022**, *12*, 12833–12844.
10. Kumar, A.; Ghalt, R.; Bal, R.; Srivastava, R. Photocatalytic  $\beta$ -O-4 bond cleavage in lignin models and native lignin through CdS integration on titanium oxide photocatalyst under visible light irradiation. *Appl. Catal. B* **2024**, *359*, 124494.
11. Lancefield, C.S.; Westwood, N.J. The synthesis and analysis of advanced lignin model polymers. *Green Chem.* **2015**, *17*, 4980–4990.
12. Pattnaik, F.; Tripathi, S.; Patra, B.; Nanda, S.; Kumar, V.; Dalai, A.; Naik, S. Catalytic conversion of lignocellulosic polysaccharides to commodity biochemicals: A review. *Environ. Chem. Lett.* **2021**, *19*, 4119–4136.
13. Kuehnle, M.; Reisner, E. Solar Hydrogen Generation from Lignocellulose. *Angew. Chem. Int. Ed.* **2018**, *57*, 3290–3296.
14. Sun, L.; Luo, N. Catalyst design and structure control for photocatalytic refineries of cellulosic biomass to fuels and chemicals. *J. Energy Chem.* **2024**, *94*, 102–127.
15. Qiu, J.; Li, M.; Ding, M.; Yao, J. Cellulose tailored semiconductors for advanced photocatalysis. *Renew. Sustain. Energy Rev.* **2022**, *154*, 111820.
16. Chan, Y.H.; Loh, S.K.; Chin, B.L.F.; Yiin, C.L.; How, B.S.; Cheah, K.W.; Wong, M.K.; Loy, A.C.M.; Gwee, Y.L.; Lo, S.L.Y.; et al. Fractionation and extraction of bio-oil for production of greener fuel and value-added chemicals: Recent advances and future prospects. *Chem. Eng. J.* **2020**, *397*, 125406.
17. Lopez, G.; Santamaria, L.; Lemonidou, A.; Zhang, S.; Wu, C.; Sipra, A.T.; Gao, N. Hydrogen generation from biomass by pyrolysis. *Nat. Rev. Method. Prim.* **2022**, *2*, 21.
18. Stevens, J.C.; Das, L.; Mobley, J.K.; Asare, S.O.; Lynn, B.C.; Rodgers, D.W.; Shi, J. Understanding laccase-ionic liquid interactions toward biocatalytic lignin conversion in aqueous ionic liquids. *ACS Sustain. Chem. Eng.* **2019**, *7*, 15928–15938.
19. Qin, Y.-Z.; Zong, M.-H.; Lou, W.-Y.; Li, N. Biocatalytic upgrading of 5-hydroxymethylfurfural (HMF) with levulinic acid to HMF Levulinate in biomass-derived solvents. *ACS Sustain. Chem. Eng.* **2016**, *4*, 4050–4054.
20. Lee, D.; Nam, H.; Won Seo, M.; Hoon Lee, S.; Tokmurzin, D.; Wang, S.; Park, Y.-K. Recent progress in the catalytic thermochemical conversion process of biomass for biofuels. *Chem. Eng. J.* **2022**, *447*, 137501.
21. Wang, H.; Liu, S.; Wang, H.; Chao, J.; Li, T.; Ellis, N.; Duo, W.; Bi, X.; Smith, K.J. Thermochemical conversion of biomass to fuels and chemicals: A review of catalysts, catalyst stability, and reaction mechanisms. *Catal. Rev.* **2023**, *67*, 57–129.
22. Duan, H.; Wang, F. Opportunities for electrocatalytic biomass valorization. *Chem. Catal.* **2022**, *2*, 641–643.
23. Lu, Y.; Yang, L.; Jiang, Y.; Yuan, Z.; Wang, S.; Zou, Y. Engineering a localized electrostatic environment to enhance hydroxyl activating for electrocatalytic biomass conversion. *Chin. J. Catal.* **2023**, *53*, 153–160.
24. Aboagye, D.; Djellabi, R.; Medina, F.; Contreras, S. Radical-mediated photocatalysis for lignocellulosic biomass conversion into value-added chemicals and hydrogen: Facts, opportunities and challenges. *Angew. Chem. Int. Ed.* **2023**, *62*, e202301909.
25. Huang, Z.; Luo, N.; Zhang, C.; Wang, F. Radical generation and fate control for photocatalytic biomass conversion. *Nat. Rev. Chem.* **2022**, *6*, 197–214.
26. Fujishima, A.; Honda, K. Electrochemical photolysis of water at a semiconductor electrode. *Nature* **1972**, *238*, 37–38.
27. Wu, Y.; Wang, H.; Li, H.; Han, X.; Zhang, M.; Sun, Y.; Fan, X.; Tu, R.; Zeng, Y.; Xu, C.C.; et al. Applications of catalysts in thermochemical conversion of biomass (pyrolysis, hydrothermal liquefaction and gasification): A critical review. *Renew. Energy* **2022**, *196*, 462–481.

28. Tawalbeh, M.; Al-Othman, A.; Salamah, T.; Alkasrawi, M.; Martis, R.; El-Rub, Z.A. A critical review on metal-based catalysts used in the pyrolysis of lignocellulosic biomass materials. *J. Environ. Manag.* **2021**, *299*, 113597.
29. Chen, H.; Wan, K.; Zheng, F.; Zhang, Z.; Zhang, Y.; Long, D. Mechanism insight into photocatalytic conversion of lignin for valuable chemicals and fuels production: A state-of-the-art review. *Renew. Sustain. Energy Rev.* **2021**, *147*, 111217.
30. You, Y.; Chen, S.; Zhao, J.; Lin, J.; Wen, D.; Sha, P.; Li, L.; Bu, D.; Huang, S. Rational design of S-scheme heterojunction toward efficient photocatalytic cellulose reforming for H<sub>2</sub> and formic acid in pure water. *Adv. Mater.* **2023**, *36*, 2307962.
31. Wang, M.; Zhou, H.; Wang, F. Photocatalytic production of syngas from biomass. *Acc. Chem. Res.* **2023**, *56*, 1057–1069.
32. Buzzetti, L.; Crisenza, G.; Melchiorre, P. Mechanistic Studies in Photocatalysis. *Angew. Chem. Int. Ed.* **2019**, *58*, 3730–3747.
33. Li, Y.; Gu, M.; Shi, T.; Cui, W.; Zhang, X.; Dong, F.; Cheng, J.; Fan, J.; Lv, K. Carbon vacancy in C<sub>3</sub>N<sub>4</sub> nanotube: Electronic structure, photocatalysis mechanism and highly enhanced activity. *Appl. Catal. B* **2020**, *262*, 118281.
34. Li, J.; Zhang, Z.; Cui, W.; Wang, H.; Cen, W.; Johnson, G.; Jiang, G.; Zhang, S.; Fong, F. The Spatially Oriented Charge Flow and Photocatalysis Mechanism on Internal van der Waals Heterostructures Enhanced g-C<sub>3</sub>N<sub>4</sub>. *ACS Catal.* **2018**, *8*, 8376–8385.
35. Cui, W.; Chen, L.; Sheng, J.; Li, J.; Wang, H.; Dong, X.; Zhou, Y.; Sun, Y.; Dong, F. The pivotal roles of spatially separated charge localization centers on themolecules activation and photocatalysis mechanism. *Appl. Catal. B* **2020**, *262*, 118251.
36. Tang, J.; Zhu, J.; Liu, L.; Xia, L.; He, Z.; Wang, D.; Xu, X.; Song, S. Coupling urchin-like TiO<sub>2</sub> nanospheres with nitrogen and sulfur co-doped graphene quantum dots for visible-light-induced degradation of toluene. *Chem. Eng. J.* **2024**, *482*, 148813.
37. Li, Z.; Wang, S.; Wu, J.; Zhou, W. Recent progress in defective TiO<sub>2</sub> photocatalysts for energy and environmental applications. *Renew. Sustain. Energy Rev.* **2022**, *156*, 111980.
38. Wu, C.; Huang, W.; Liu, H.; Lv, K.; Li, Q. Insight into synergistic effect of Ti<sub>3</sub>C<sub>2</sub> MXene and MoS<sub>2</sub> on anti-photocorrosion and photocatalytic of CdS for hydrogen production. *Appl. Catal. B* **2023**, *330*, 122653.
39. Wang, X.; Maeda, K.; Thomas, A.; Takanabe, K.; Xin, G.; Carlsson, J.M.; Domen, K.; Antonietti, M. A metal-free polymeric photocatalyst for hydrogen production from water under visible light. *Nat. Mater.* **2008**, *8*, 76–80.
40. Yue, J.; Yang, H.; Liu, C.; Wang, S.; Kang, X. In-plane electron transfer dominated carbon nitride for high-efficiency quasi-homogeneous photochemical synthesis of hydrogen peroxide. *Chem. Eng. J.* **2024**, *497*, 154683.
41. Abdellatif, H.; Zhang, G.; Wang, X.; Xie, D.; Irvine, J.; Ni, J.; Ni, C. Boosting photocatalytic oxidation on graphitic carbon nitride for efficient photocatalysis by heterojunction with graphitic carbon units. *Chem. Eng. J.* **2019**, *370*, 874–884.
42. Xu, C.; Liu, H.; Wang, D.; Li, D.; Zhang, Y.; Liu, X.; Huang, J.; Wu, S.; Fan, D.; Liu, H.; et al. Molten-salt assisted synthesis of polymeric carbon nitride-based photocatalyst for enhanced photocatalytic activity under green light irradiation. *Appl. Catal. B* **2023**, *334*, 122835.
43. Yang, H.; Zhou, Y.; Wang, Y.; Hu, S.; Wang, B.; Liao, Q.; Li, H.; Bao, J.; Ge, G.; Jia, S. Three-dimensional flower-like phosphorus-doped g-C<sub>3</sub>N<sub>4</sub> with a high surface area for visible-light photocatalytic hydrogen evolution. *J. Mater. Chem. A* **2018**, *6*, 16485–16494.
44. Aggarwal, M.; Basu, S.; Shetti, N.P.; Nadagouda, M.N.; Kwon, E.E.; Park, Y.-K.; Aminabhavi, T.M. Photocatalytic carbon dioxide reduction: Exploring the role of ultrathin 2D graphitic carbon nitride (g-C<sub>3</sub>N<sub>4</sub>). *Chem. Eng. J.* **2021**, *425*, 131402.
45. Chen, M.; Sun, M.; Cao, X.; Wang, H.; Xia, L.; Jiang, W.; Huang, M.; He, L.; Zhao, X.; Zhou, Y. Progress in preparation, identification and photocatalytic application of defective g-C<sub>3</sub>N<sub>4</sub>. *Coord. Chem. Rev.* **2024**, *51*, 215849.
46. Huang, Q.-S.; Li, Q.; Chu, C.; Liu, Q.; Li, Z.; Mao, S. Synergetic regulation of electronic structure of graphitic carbon nitride through phosphorus and carbon co-doping for enhanced photocatalytic CO<sub>2</sub> reduction. *Chem. Eng. J.* **2024**, *428*, 149155.
47. You, Q.; Zhang, C.; Cao, M.; Wang, B.; Huang, J.; Wang, Y.; Deng, S.; Yu, G. Defects controlling, elements doping, and crystallinity improving triple-strategy modified carbon nitride for efficient photocatalytic diclofenac degradation and H<sub>2</sub>O<sub>2</sub> production. *Appl. Catal. B* **2023**, *321*, 121941.
48. Guo, L.; Gao, J.; Huang, Q.; Wang, X.; Li, Z.; Li, M.; Zhou, W. Element engineering in graphitic carbon nitride photocatalysts. *Renew. Sust. Energ. Rev.* **2024**, *199*, 114482.
49. Zhao, D.; Guan, X.; Shen, S. Design of polymeric carbon nitride-based heterojunctions for photocatalytic water splitting: A review. *Environ. Chem. Lett.* **2022**, *20*, 3505–3523.
50. Luo, M.; Jiang, G.; Yu, M.; Yan, Y.; Qin, Z.; Li, Y.; Zhang, Q. Constructing crystalline homophase carbon nitride S-scheme heterojunctions for efficient photocatalytic hydrogen evolution. *J. Mater. Sci. Technol.* **2023**, *161*, 220–232.
51. Akinaga, Y.; Kawawaki, T.; Kameko, H.; Yamazaki, Y.; Yamazaki, K.; Nakayasu, Y.; Kato, K.; Tanaka, Y.; Hanindriyo, A.T.; Takagi, M.; et al. Metal single-atom cocatalyst on carbon nitride for the photocatalytic hydrogen evolution reaction: Effects of metal species. *Adv. Funct. Mater.* **2023**, *33*, 2303321.
52. Li, K.; Lin, Y.-Z.; Wang, K.; Wang, Y.; Zhang, Y.; Zhang, Y.; Liu, F.-T. Rational design of cocatalyst system for improving the photocatalytic hydrogen evolution activity of graphite carbon nitride. *Appl. Catal. B* **2020**, *268*, 118402.
53. Liu, Y.; He, M.; Guo, R.; Fang, Z.; Kang, S.; Ma, Z.; Dong, M.; Wang, W.; Cui, L. Ultrastable metal-free near-infrared-driven photocatalysts for H<sub>2</sub> production based on protonated 2D g-C<sub>3</sub>N<sub>4</sub> sensitized with Chlorin e6. *Appl. Catal. B* **2020**,

- 260, 118137.
54. Zhang, X.; Yu, L.; Zhuang, C.; Peng, T.; Li, R.; Li, X. Highly asymmetric phthalocyanine as a sensitizer of graphitic carbon nitride for extremely efficient photocatalytic H<sub>2</sub> production under near-infrared light. *ACS Catal.* **2013**, *4*, 162–170.
  55. Ong, W.-J.; Tan, L.-L.; Ng, Y.H.; Yong, S.-T.; Chai, S.-P. Graphitic carbon nitride (g-C<sub>3</sub>N<sub>4</sub>)-based photocatalysts for artificial photosynthesis and environmental remediation: Are we a step closer to achieving sustainability? *Chem. Rev.* **2016**, *116*, 7159–7329.
  56. Wen, J.; Xie, J.; Chen, X.; Li, X. A review on g-C<sub>3</sub>N<sub>4</sub>-based photocatalysts. *Appl. Surf. Sci.* **2017**, *391*, 72–123.
  57. Ding, L.-L.; Ge, J.-P.; Zhou, W.-Q.; Gao, J.-P.; Zhang, Z.-Y.; Xiong, Y. Nanogold-functionalized g-C<sub>3</sub>N<sub>4</sub> nanohybrids for sensitive impedimetric immunoassay of prostate-specific antigen using enzymatic biocatalytic precipitation. *Biosens. Bioelectron.* **2016**, *85*, 212–219.
  58. Liu, R.; Lin, J.; Zhu, L.; Zhang, X.; Li, Y.; Pan, H.; Kong, L.; Zhu, S.; Wang, J. Synergistic effect of donor-acceptor structure and built-in electric field in hollow-spherical carbon nitride homojunction towards effective charge transfer and excellent photocatalytic hydrogen evolution performance. *Chem. Eng. J.* **2024**, *484*, 149507.
  59. Tang, C.; Cheng, M.; Lai, C.; Li, L.; Yang, X.; Du, L.; Zhang, G.; Wang, G.; Yang, L. Recent progress in the applications of non-metal modified graphitic carbon nitride in photocatalysis. *Coord. Chem. Rev.* **2023**, *474*, 214846.
  60. Jiang, L.; Yuan, X.; Pan, Y.; Liang, J.; Zeng, G.; Wu, Z.; Wang, H. Doping of graphitic carbon nitride for photocatalysis: A review. *Appl. Catal. B* **2017**, *217*, 388–406.
  61. Ma, J.; Li, X.; Li, Y.; Jiao, G.; Su, H.; Xiao, D.; Zhai, S.; Sun, R. Single-atom zinc catalyst for co-production of hydrogen and fine chemicals in soluble biomass solution. *Adv. Powder Mater.* **2022**, *1*, 100058.
  62. Wang, E.; Mahmood, A.; Chen, S.-G.; Sun, W.; Muhmood, T.; Yang, X.; Chen, Z. Solar-driven photocatalytic reforming of lignocellulose into H<sub>2</sub> and value-added biochemicals. *ACS Catal.* **2022**, *12*, 11206–11215.
  63. Huang, Z.; Sun, P.; Liu, H.; Ren, C.; Lin, X.; Shen, M.; Li, Z.; Xu, X. Efficient selective cleavage of C–C bonds in lignin under visible light enabled by the Fe-doped mesoporous graphitic carbon nitride photocatalyst. *Ind. Crop. Prod.* **2024**, *222*, 119642.
  64. Wang, J.; Zhao, Q.; Kumar, P.; Zhao, H.; Jing, L.; Di Tommaso, D.; Crespo-Otero, R.; Kibria, M.G.; Hu, J. Solar-driven cellulose photorefining into arabinose over oxygen-doped carbon nitride. *ACS Catal.* **2024**, *14*, 3376–3386.
  65. Liu, K.; Ma, J.; Yang, X.; Liu, Z.; Li, X.; Zhang, J.; Cui, R.; Sun, R. Phosphorus/oxygen co-doping in hollow-tube-shaped carbon nitride for efficient simultaneous visible-light-driven water splitting and biorefinery. *Chem. Eng. J.* **2022**, *437*, 135232.
  66. LeBlanc, G.; Chen, G.; Gizzie, E.A.; Jennings, G.K.; Cliffler, D.E. Enhanced photocurrents of photosystem I films on p-doped silicon. *Adv. Mater.* **2012**, *24*, 5959–5962.
  67. Yang, X.; Ma, J.; Sun, S.; Liu, Z.; Sun, R. K/O co-doping and introduction of cyano groups in polymeric carbon nitride towards efficient simultaneous solar photocatalytic water splitting and biorefineries. *Green Chem.* **2022**, *24*, 2104–2113.
  68. Gao, H.; Yan, S.; Wang, J.; Huang, Y.A.; Wang, P.; Li, Z.; Zou, Z. Towards efficient solar hydrogen production by intercalated carbon nitride photocatalyst. *Phys. Chem. Chem. Phys.* **2013**, *15*, 18077.
  69. Tahir, M.; Sherryana, A.; Khan, A.A.; Madi, M.; Zerga, A.Y.; Tahir, B. Defect engineering in graphitic carbon nitride nanotextures for energy efficient solar fuels production: A review. *Energy Fuels* **2022**, *36*, 8948–8977.
  70. Maarisetty, D.; Baral, S.S. Defect engineering in photocatalysis: Formation, chemistry, optoelectronics, and interface studies. *J. Mater. Chem. A* **2020**, *8*, 18560–18604.
  71. Zou, R.; Chen, Z.; Zhong, L.; Yang, W.; Li, T.; Gan, J.; Yang, Y.; Chen, Z.; Lai, H.; Li, X.; et al. Nanocellulose-assisted molecularly engineering of nitrogen deficient graphitic carbon nitride for selective biomass photo-oxidation. *Adv. Funct. Mater.* **2023**, *33*, 2301311.
  72. Zhao, C.; Shi, C.; Li, Q.; Wang, X.; Zeng, G.; Ye, S.; Jiang, B.; Liu, J. Nitrogen vacancy-rich porous carbon nitride nanosheets for efficient photocatalytic H<sub>2</sub>O<sub>2</sub> production. *Mater. Today Energy* **2022**, *24*, 100926.
  73. Bai, X.; Hou, Q.; Qian, H.; Nie, Y.; Xia, T.; Lai, R.; Yu, G.; Laiq Ur Rehman, M.; Xie, H.; Ju, M. Selective oxidation of glucose to gluconic acid and glucaric acid with chlorin e6 modified carbon nitride as metal-free photocatalyst. *Appl. Catal. B* **2022**, *303*, 120895.
  74. Yu, H.; Shi, R.; Zhao, Y.; Bian, T.; Zhao, Y.; Zhou, C.; Waterhouse, G.I.N.; Wu, L.Z.; Tung, C.H.; Zhang, T. Alkali-assisted synthesis of nitrogen deficient graphitic carbon nitride with tunable band structures for efficient visible-light-driven hydrogen evolution. *Adv. Mater.* **2017**, *29*, 1605148.
  75. Chen, C.-C.; Tsai, D.-L.; Liu, H.-T.; Wu, J.-J. Carbon Vacancy-Modified Carbon Nitride Allotropic Composite for Solar Hydrogen Generation Coupled with Selective Oxidation of 5-Hydroxymethylfurfural. *ACS Sustain. Chem. Eng.* **2023**, *11*, 6435–6444.
  76. Du, X.; Zhang, H.; Yao, T.; Dong, S.; Jing, L.; Hu, J. Cyano and defective co-modified carbon nitride for optimized photoreformation of glucose to arabinose. *Surf. Interfaces* **2024**, *48*, 104283.
  77. Cao, M.; Shao, S.; Wei, W.; Love, J.; Yue, Z.; Zhang, Y.; Zhang, X.; Xue, Y.; Yu, J.; Fan, X. Engineering multiple defect sites on ultrathin graphitic carbon nitride for efficiently photocatalytic conversion of lignin into monomeric aromatics via

- selective C–C bond scission. *Appl. Surf. Sci.* **2024**, *643*, 158653.
78. Mitchell, E.; Law, A.; Godin, R. Interfacial charge transfer in carbon nitride heterojunctions monitored by optical methods. *J. Photochem. Photobiol. C Photochem. Rev.* **2021**, *49*, 100453.
79. Deng, A.; Sun, Y.; Gao, Z.; Yang, S.; Liu, Y.; He, H.; Zhang, J.; Liu, S.; Sun, H.; Wang, S. Internal electric field in carbon nitride-based heterojunctions for photocatalysis. *Nano Energy* **2023**, *108*, 108228.
80. Uekert, T.; Kasap, H.; Reisner, E. Photoreforming of nonrecyclable plastic waste over a carbon nitride/nickel phosphide catalyst. *J. Am. Chem. Soc.* **2019**, *141*, 15201–15210.
81. Xu, Q.; Zhang, L.; Cheng, B.; Fan, J.; Yu, J. S-scheme heterojunction photocatalyst. *Chem* **2020**, *6*, 1543–1559.
82. Ling, W.; Ma, J.; Hong, M.; Sun, R. Enhance photocatalytic CO<sub>2</sub> reduction and biomass selective oxidation via sulfur vacancy-enriched S-scheme heterojunction of MoS<sub>2</sub>@GCN. *Chem. Eng. J.* **2024**, *493*, 152729.
83. Wu, G.; Wu, Z.; Liu, L.; Cui, W.; Du, D.; Xue, Y. NIR light responsive MoS<sub>2</sub> nanomaterials for rapid sterilization: Optimum photothermal effect via sulfur vacancy modulation. *Chem. Eng. J.* **2022**, *427*, 132007.
84. Xu, X.; Dai, S.; Xu, S.; Zhu, Q.; Li, Y. Efficient photocatalytic cleavage of lignin models by a soluble perylene diimide/carbon nitride S-scheme heterojunction. *Angew. Chem. Int. Ed.* **2023**, *62*, e202309066.
85. Cai, M.; Liu, Y.; Dong, K.; Chen, X.; Li, S. Floatable S-scheme Bi<sub>2</sub>WO<sub>6</sub>/C<sub>3</sub>N<sub>4</sub>/carbon fiber cloth composite photocatalyst for efficient water decontamination. *Chin. J. Catal.* **2023**, *52*, 239–251.
86. Zhang, J.; Yu, J.; Yang, C.; Li, S. Recent progress on S-scheme heterojunction strategy enabling polymer carbon nitrides C<sub>3</sub>N<sub>4</sub> and C<sub>3</sub>N<sub>5</sub> enhanced photocatalysis in energy conversion and environmental remediation. *Curr. Opin. Chem. Eng.* **2024**, *45*, 101040.
87. Ding, Y.; Cao, Y.; Chen, D.; Li, J.; Wu, H.; Meng, Y.; Huang, J.; Yuan, J.; Su, Y.; Wang, J.; et al. Relay photo/thermal catalysis enables efficient cascade upgrading of sugars to lactic acid: Mechanism study and life cycle assessment. *Chem. Eng. J.* **2023**, *452*, 139687.
88. Chen, Y.; Qu, Y.; Xu, P.; Zhou, X.; Sun, J. Insight into the influence of donor-acceptor system on graphitic carbon nitride nanosheets for transport of photoinduced charge carriers and photocatalytic H<sub>2</sub> generation. *J. Colloid Interface Sci.* **2021**, *601*, 326–337.
89. Qian, Y.; Han, Y.; Zhang, X.; Yang, G.; Zhang, G.; Jiang, H.-L. Computation-based regulation of excitonic effects in donor-acceptor covalent organic frameworks for enhanced photocatalysis. *Nat. Commun.* **2023**, *14*, 3083.
90. Lan, Z.A.; Zhang, G.; Chen, X.; Zhang, Y.; Zhang, K.A.I.; Wang, X. Reducing the exciton binding energy of donor-acceptor-based conjugated polymers to promote charge-induced reactions. *Angew. Chem. Int. Ed.* **2019**, *58*, 10236–10240.
91. Ou, H.; Chen, X.; Lin, L.; Fang, Y.; Wang, X. Biomimetic donor-acceptor motifs in conjugated polymers for promoting exciton splitting and charge separation. *Angew. Chem. Int. Ed.* **2018**, *57*, 8729–8733.
92. Liu, J.; Zou, R.; Zhang, H.; Song, Y.; Liu, Y.; Yang, S.; Xia, R.; Iwuoha, E.I.; Feloni, U.; Admassie, S.; Peng, X. Enhanced  $\pi$ -electron transport in graphitic carbon nitride (g-C<sub>3</sub>N<sub>4</sub>) by constructing biochar-welded donor-acceptor (D-A) configuration for photocatalytic conversion of biomass. *Appl. Catal. B* **2024**, *357*, 124312.
93. Li, X.; Wu, Y.; Zhang, S.; Cai, B.; Gu, Y.; Song, J.; Zeng, H. CsPbX<sub>3</sub> quantum dots for lighting and displays: Room-temperature synthesis, photoluminescence superiorities, underlying origins and white light-emitting diodes. *Adv. Funct. Mater.* **2016**, *26*, 2435–2445.
94. Ling, W.; Ma, J.; Liu, Z.; Cui, R.; Zhang, J.; Li, X.; Hong, M.; Sun, R. Enhancing biomass oxidation with carbon nitride nanosheets ring inserted on CI Pigment Yellow 53 photocatalysts for simultaneous CO and lactic acid production. *Chem. Eng. J.* **2023**, *475*, 146117.
95. Jiang, Z.; Wang, B.; Yu, J.C.; Wang, J.; An, T.; Zhao, H.; Li, H.; Yuan, S.; Wong, P.K. AgInS<sub>2</sub>/In<sub>2</sub>S<sub>3</sub> heterostructure sensitization of Escherichia coli for sustainable hydrogen production. *Nano Energy* **2018**, *46*, 234–240.
96. Hu, A.; Ye, J.; Ren, G.; Qi, Y.; Chen, Y.; Zhou, S. Metal-free semiconductor-based bio-nano hybrids for sustainable CO<sub>2</sub>-to-CH<sub>4</sub> conversion with high quantum yield. *Angew. Chem. Int. Ed.* **2022**, *61*, e202206508.
97. Sakimoto, K.K.; Wong, A.B.; Yang, P. Self-photosensitization of nonphotosynthetic bacteria for solar-to-chemical production. *Science* **2016**, *351*, 74–77.
98. Ye, J.; Chen, Y.; Gao, C.; Wang, C.; Hu, A.; Dong, G.; Chen, Z.; Zhou, S.; Xiong, Y. Sustainable conversion of microplastics to methane with ultrahigh selectivity by a biotic-abiotic hybrid photocatalytic system. *Angew. Chem. Int. Ed.* **2022**, *61*, e202213244.
99. Hou, M.; Wang, R.; Wu, X.; Zhang, Y.; Ge, J.; Liu, Z. Synthesis of lutein esters by using a reusable lipase-Pluronic conjugate as the catalyst. *Catal. Lett.* **2015**, *145*, 1825–1829.
100. Xu, M.; Tremblay, P.-L.; Jiang, L.; Zhang, T. Stimulating bioplastic production with light energy by coupling *Ralstonia eutropha* with the photocatalyst graphitic carbon nitride. *Green Chem.* **2019**, *21*, 2392–2400.
101. Wang, J.; Xu, M.; Tremblay, P.-L.; Zhang, T. Improved polyhydroxybutyrate production by *Cupriavidus necator* and the photocatalyst graphitic carbon nitride from fructose under low light intensity. *Int. J. Biol. Macromol.* **2022**, *203*, 526–534.
102. Nasir, M.S.; Yang, G.; Ayub, I.; Wang, S.; Wang, L.; Wang, X.; Yan, W.; Peng, S.; Ramakarishna, S. Recent development in

- graphitic carbon nitride based photocatalysis for hydrogen generation. *Appl. Catal. B* **2019**, *257*, 117855.
103. Chen, F.; Wu, C.; Zheng, G.; Qu, L.; Han, Q. Few-layer carbon nitride photocatalysts for solar fuels and chemicals: Current status and prospects. *Chin. J. Catal.* **2022**, *43*, 1216–1229.
  104. Ma, J.; Liu, K.; Yang, X.; Jin, D.; Li, Y.; Jiao, G.; Zhou, J.; Sun, R. Recent advances and challenges in photoreforming of biomass-derived feedstocks into hydrogen, biofuels, or chemicals by using functional carbon nitride photocatalysts. *ChemSusChem* **2021**, *14*, 4903–4922.
  105. Qiang, G.; Ansari, M.; Sun, Z.; Elangovan, S. Bioactive Molecules from Lignocellulose-Derived Platform Chemicals. *Adv. Synth. Catal.* **2024**, *366*, 4805–4834.
  106. Tiwari, M.S.; Wagh, D.; Dicks, J.S.; Keogh, J.; Ansaldi, M.; Ranade, V.V.; Manyar, H.G. Solvent free upgrading of 5-hydroxymethylfurfural (HMF) with levulinic acid to HMF levulinate using tin exchanged tungstophosphoric acid supported on K-10 catalyst. *ACS Org. Inorg. Au* **2022**, *3*, 27–34.
  107. Lucarelli, C.; Vaccari, A. Examples of heterogeneous catalytic processes for fine chemistry. *Green Chem.* **2011**, *13*, 1941–1949.
  108. Blaser, H.-U.; Studer, M. The role of catalysis for the clean production of fine chemicals. *Appl. Catal. A* **1999**, *189*, 191–204.